Fusion Engineering and Design 202 (2024) 114321

Contents lists available at ScienceDirect

Fusion Engineering and Design

journal homepage: www.elsevier.com/locate/fusengdes

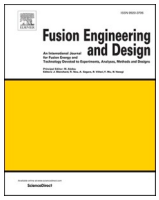

# Analysis of the integral zeolite molecular sieve process for helium CPS application

Vincenzo Narcisi *, Alessia Santucci

*ENEA, Fusion and Technology for Nuclear Safety and Security Department, Via E. Fermi 45, 00044 Frascati RM, Italy*

ARTICLE INFO

*Keywords:*
Process simulation
Tritiated water capture
Fuel cycle
DEMO
Coolant purification system

ABSTRACT

Zeolite Molecular Sieves (ZMSs) are commonly adopted in tritium handling facilities for impurity removal from gaseous streams, particularly for tritiated water trapping. Several activities have been conducted to characterize the adsorption and desorption behaviour of the sieving materials. Instead, less attention has been put on the analysis of the integral process comprising the adsorption of the tritiated humidity, the regeneration of the molecular sieve and the recovery of the desorbed water. Focusing on the application for the EU-DEMO helium Coolant Purification System (CPS), this work presents a process simulator relying on a MATLAB dynamic model of the ZMS bed and on a RELAP5/MOD3.3 model for the regeneration loop. The dynamic model can simulate both the adsorption and regeneration modes of the ZMS by providing the temperature and the adsorbate concentration profile along the column, while the thermal-hydraulic model is used to assess the conditions of the regeneration loop. By coupling the outcomes of the two models it is possible to establish the effective regeneration efficiency of the process and the amount of the tritiated water recovered. For the case of helium CPS, the analysis demonstrates the feasibility of the proposed operative scheme and the capabilities of the regeneration procedure to ensure a 74.4 % regeneration efficiency of the ZMS bed.

## 1. Introduction

Adsorption is a widely used method in processes where removal of impurities from chemicals and solvents is required to produce ultra-pure components. The pharmaceutical and the oil and gas industries are typical examples where some products need to be exceedingly pure and removal of water is essential to prevent its freezing in the cryogenic processes [1,2]. For all these applications, ZMS are the preferred adsorbent media for an efficient water removal [1–4]. Among these, Zeolite A, typically 4A, represents the most used molecular sieve for dehydration of gases, thanks to its strong adsorption capabilities for water at low concentrations. Alternatively, if the coadsorption of $CO_2$ must be avoided, molecular sieve 3A should be preferred over 4A [2]. Once saturated (i.e., the equilibrium between water molecules in the adsorbent solid phase and water molecules dispersed in the gaseous stream is reached) the ZMS bed must be regenerated, meaning that the adsorption capabilities of the bed must return to the original state. In the Pressure Swing Adsorption (PSA) process, once the bed is saturated, the water partial pressure is reduced in the gas phase allowing the release of the adsorbed water, whereas in the Temperature Swing Adsorption (TSA) the same effect is obtained by increasing the temperature of the adsorbent material [2]. Both the methodologies involve the presence of a purge gas stream (typically 10–15 % of the adsorption throughput), where the released water constitutes the humidity content in the regeneration stream. Normally, the industrial processes do not pose particular attention to this stream, instead for other applications, as the fusion ones, its management and treatment is of great relevance, being the contained water tritiated. As a matter of fact, ZMS beds are frequently adopted in tritium handling facilities to collect and recover traces of tritiated water from a given gas stream [5], and their use is foreseen also in the fuel cycle of future fusion machines, as the EU-DEMO.

The EU-DEMO is the European demonstrator of a Fusion Power Plant (FPP) that has to prove the possibility of net electricity production and tritium self-sufficiency of future FPPs. A central role is played by the Breeding Blanket (BB), representing one of the most innovative components and the step forward from ITER to the future FPPs [6]. Among other functionalities, the BB must ensure an efficient delivering towards the Primary Heat Transport System (PHTS) of the power deposited by neutrons and must guarantee a proper tritium breeding for the self-sufficiency of the machine. To do this, large and thin metallic

* Corresponding author.
*E-mail address:* vincenzo.narcisi@enea.it (V. Narcisi).

https://doi.org/10.1016/j.fusengdes.2024.114321
Received 31 January 2024; Received in revised form 1 March 2024; Accepted 5 March 2024
Available online 11 March 2024

**List of acronyms**

| | |
|---|---|
| BB | Breeding Blanket |
| CCWS | Component Cooling Water System |
| CPS | Coolant Purification System |
| FPP | Fusion Power Plant |
| HCPB | Helium-Cooled Pebble Bed |
| LDF | Linear Driving Force |
| LWR | Light Water Reactor |
| NEG | Non-Evaporable Getter |
| NRC | Nuclear Regulatory Commission |
| OD | Outside Diameter |
| PFD | Process Flow Diagram |
| PHTS | Primary Heat Transport System |
| PSA | Pressure Swing Adsorption |
| TBM | Test Blanket Module |
| TSA | Temperature Swing Adsorption |
| WCLL | Water-Cooled Lithium Lead |
| WDS | Water Detritiation System |
| ZMS | Zeolite Molecular Sieve |

surfaces and high temperatures are employed for the heat transfer, and high tritium concentrations are expected for the tritium self-sufficiency. Such operative conditions pose the basis for the chronical tritium permeation from BB to PHTS and so, for the issue of the tritium migration towards rooms and environment [7].

The mitigation strategy adopted to limit the tritium migration from BB relies on the adoption of anti-permeation barriers, applied to metallic surfaces, and of the Coolant Purification System (CPS), designed to keep a target tritium concentration in the primary coolant according to safety considerations and to recover tritium for its reuse as fuel [8,9]. Focusing on the CPS, the employed technology for the tritium recovery depends on the coolant medium. Currently, two BB concepts are under investigation for the EU-DEMO, namely the Helium-Cooled Pebble Bed (HCPB) and the Water-Cooled Lithium Lead (WCLL) [10]. The present paper is focused on the HCPB in which helium at 8 MPa is used as coolant (300 °C-520 °C is the BB temperature window), lithium is the breeder, and beryllium the neutron multiplier [10].

In the frame of the EU-DEMO pre-concept design, two technologies were individuated for the HCPB BB CPS (called helium CPS in the following). The more conventional solution is based on industrial processes already used in fission plants and foreseen for the ITER HCPB Test Blanket Module (TBM), where all the hydrogen isotopes contained in the primary coolant are burned in Copper Oxide (CuO) beds and the formed water adsorbed through Zeolite Molecular Sieve (ZMS) beds. The other one is the most innovative technology based on novel Non-Evaporable Getter (NEG) beds for the direct adsorption of hydrogen isotopes, bypassing the formation of water [8]. Although R&D continues for both the technologies, the one relying on CuO and ZMS beds is currently considered the reference for the EU-DEMO helium CPS, being the most mature process. As such, the present paper deals with the advancement in the design of this solution posing attention on the regeneration procedure of the ZMS that presents new peculiarities related to the tritium management.

In the pre-concept design phase, a closed ZMS regeneration loop was conceived where the tritium recovery function is fulfilled by a condenser, removing as much humidity as possible from the regeneration purge stream [11]. The novelty of the present work is the assessment of the procedure and the performance of the ZMS regeneration. Such an analysis is performed on the EU-DEMO helium CPS, but the outcomes can be extrapolated whenever ZMS are used to recover tritiated water from gaseous streams.

## 2. Interfaces and preliminary dimensioning

The schematic view of the helium CPS based on CuO and ZMS beds, along with its interfaces with the PHTS, is presented in Fig. 1.

A small fraction of the primary coolant throughput, consisting in helium plus trace of hydrogen ($Q_2$ in Fig. 1, where Q stands for the three isotopes H, D, and T), is withdrawn downstream the compressor of the Primary Heat Transport System and routed into the CuO beds where $Q_2$ is burned into $Q_2O$ at 300 °C. The resulting stream passes through the economizer and the chiller to reach ambient temperature required for the water adsorption in the ZMS bed. Almost all the $Q_2O$ content is recovered, and the purified helium returns to the PHTS after restoring its temperature through the economizer. Both the CuO and the ZMS beds works in batch operation thus, the regeneration loops ensure the restore of the oxidizing and adsorption capabilities of the CuO and ZMS beds, respectively.

In terms of tritium inventory, the Zeolite Molecular Sieve bed and the relative regeneration loop are the most relevant sub-systems of the helium CPS. For this reason, the activity presented in this paper is mainly focused on the preliminary dimensioning of the ZMS beds and on the regeneration process to be adopted for the final recovery of tritium.

The procedure for the preliminary dimensioning of the beds is derived from the work of Tosti et al. [14] and the main parameters assumed for the calculation are collected in Table 1. Regarding the protium addition into primary coolant, it's amount has been established to dilute the tritiated water coming from the ZMS regeneration to the value of 100 Ci $kg^{-1}$, being the target concentration for the EU-DEMO Water Detritiation System (WDS) [16]. Further requirements on this parameter could emerge in the future related to the coolant chemistry.

The sizing procedure starts with the calculation of the primary flow rate to be routed to the Coolant Purification System ($F_{CPS}$) in order to keep the target HT concentration ($c_0$) into PHTS with the imposed BB tritium permeation ($F_{T,p}$) [8]:

$$F_{CPS} = \frac{F_{T,p}}{\eta_{CPS}\left(c_0 - \frac{F_{T,p}}{F_{PHTS}}\right)} \tag{1}$$

In Eq. (1), $F_{PHTS}$ is the total PHTS flow rate (1777.76 kg $s^{-1}$ [12]) and $\eta_{CPS}$ is the detritiation efficiency of the entire CPS, defined as the ratio between the moles of tritium recovered by and entering the CPS. Although a $\eta_{CPS}$ close to 100 % is expected, a conservative value of 90 % is considered and the helium flow rate to be routed into CPS is calculated

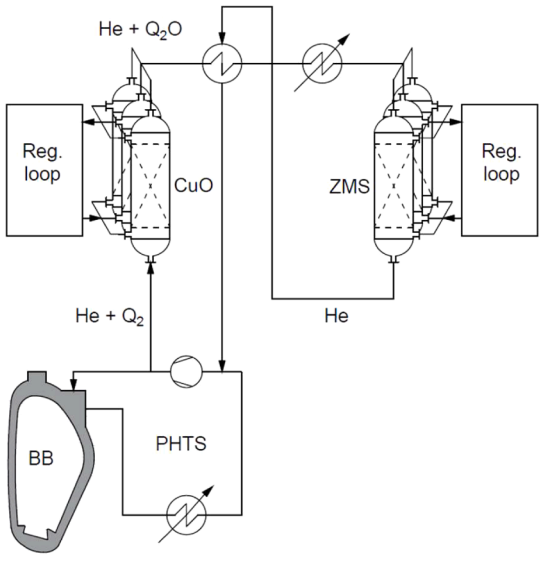


**Fig. 1.** Schematic view of the helium CPS relying on CuO and ZMS beds and interface with PHTS.

**Table 1**
Main parameters adopted for the preliminary dimensioning of the ZMS beds.

| Parameter | Unit | Value | Reference |
|---|---|---|---|
| Helium pressure | MPa | 8 | [12] |
| C uO oxidizing temperature | °C | 300 | [13] |
| Z MS adsorption temperature | °C | 25 | [14] |
| Z MS regeneration temperature | °C | 300 | [14] |
| BB tritium permeation | g $d^{-1}$ | 0.36 | [15] |
| Target HT partial pressure in PHTS | Pa | 0.04 | [8] |
| Protium addition to primary coolant | Pa | 640 | – |

equal to 1.297 kg $s^{-1}$ (around 0.7 % of the primary flow rate). The bed dimensions are obtained by evaluating the maximum superficial velocity $u$ (defined as the velocity through the empty bed) and then, the minimum bed diameter. Actual diameter is obtained applying a margin of 10 % to the minimum value whereas the bed heigh is calculated with a length to diameter ratio of 1.5. The maximum superficial velocity is evaluated with the Ergun's equation [17]:

$$\frac{\Delta p}{L} = \frac{150(1-\varepsilon)^2}{D_p^2\ \varepsilon^3}\mu u + \frac{1.75(1-\varepsilon)}{D_p\ \varepsilon^3}\rho u^2 \tag{2}$$

where $\varepsilon$ is the bed void fraction assumed equal to 0.37, $D_p$ the particle diameter (1.6 mm), $\mu$ the coolant dynamic viscosity, $\rho$ the coolant density, and $\Delta p\ L^{-1}$ is the allowable linear pressure assumed equal to 7.5 kPa $m^{-1}$ for the ZMS bed [14]. The number of beds in simultaneous adsorption mode and their most relevant features are summarized in Table 2.

## 3. Regeneration of the ZMS bed

Fig. 2 presents the proposed schedule for the adsorption and regeneration of the ZMS beds involved in the operation of the EU-DEMO helium CPS, where green, red, and blue arrows represent the adsorption, the regeneration, and the standby phases, respectively. As a matter of fact, the regeneration process is expected to be faster than the adsorption and thus, one regenerated the bed is kept in standby conditions waiting for the subsequent adsorption phase. The characteristic times are individuated by $t$, where the superscripts indicate the beds in adsorption mode and the subscripts indicate the beginning of the regeneration (*0*) or of the standby (*1*) of the remaining bed.

As reported in Table 2, two ZMS beds in simultaneous adsorption mode are foreseen for the helium CPS and so, at least three beds are needed to ensure the continuous operation, being the third in regeneration mode. The verification of the possibility to implement the schedule proposed in Fig. 2 is one of the objectives of the present work.

The regeneration loop has been preliminary designed and simulation activities has been performed to test capabilities of the system. Fig. 3 presents the Process Flow Diagram (PFD) of the ZMS regeneration loop. Once saturated, the ZMS bed is isolated from the adsorption loop with valves v-01 and v-02. Valves v-03 and v-04 open allowing the circulation of the regeneration stream. This stream consists of a small flow rate of purge helium (typically between 10 % and 15 % of the adsorption flow rate) plus residual humidity coming from the previous regeneration. Exiting the ZMS-01, the mixture is sent to the hot side of the economizer (ECO-01), where the temperature is reduced while preventing condensation of the humidity. It is envisaged condensing humidity only inside the condenser (CND-01), where the condensate can be collected. For this reason, a moisture controller monitors the thermodynamic conditions at the outlet of the ECO-01 hot side regulating the power of the heater HT-01 that ensures an inlet temperature at the ECO-01 cold side higher than the dew point at the outlet of the ECO-01 hot side. Then, the mixture goes into the CND-01 where most of the humidity is condensed and collected inside the drum (DR-01). A controlled water flow rate can be sent from the DR-01 to the WDS for further processing. The helium plus residual humidity is sent to the HT-01, passes through the ECO-01 cold side and, before entering the ZMS bed, is warmed in the second heater (HT-02) to restore required conditions for the regeneration (i.e., 300 °C). The residual humidity is an important figure of merit of the system since it determines the achievable regeneration efficiency of the ZMS bed and the baseline tritium inventory inside the regeneration loop.

**Table 2**
Preliminary dimensioning of the ZMS beds.

| Parameter | Unit | Value |
|---|---|---|
| Number of beds in adsorption mode | – | 2 |
| Bed diameter | m | 0.753 |
| Bed length | m | 1.129 |
| Pressure drops | kPa | 3.7 |
| Total tritium inventory before regeneration | g | 1.2 |

Once regenerated, ZMS-01 is isolated from the regeneration loop by closing v-03 and v-04 and kept in standby until the subsequent adsorption phase. At the same time, v-05 opens and the recirculation loop continues to work in steady state conditions, keeping the system ready for the following regeneration.

The ECO-01 is a hairpin heat exchanger whereas the CND-01 and the two heaters are shell and tubes heat exchanger. The CND-01 is supposed to be cooled by a Component Cooling Water System (CCWS) at 15 °C (CND-01 tube side) whereas HT-01 and HT-02 are equipped with electrically heated pins. The main features of the heat exchangers are reported in Table 3.

The pipeline is characterized by an Outside Diameter (OD) of 0.1413 m and the total length is preliminary assumed equal to 16.5 m. It is worth mentioning that the footprint of the system is not defined yet thus, length and numbers of bends (37 90° bends are supposed in this work) are preliminary assumed for the preliminary thermal-hydraulic simulations. The structural material is austenitic steel, and the thickness has been evaluated with ASME Sect. III NC [18] according to the design parameters of the PHTS [12].

### 3.1. Modelling

A process simulator of the Zeolite Molecular Sieve regeneration system has been developed, dividing it in two domains. The ZMS bed is simulated with a dynamic model developed in MATLAB whereas the regeneration loop is modelled with RELAP5/MOD3.3. The interfaces, through which the models exchange boundary conditions, are represented by the valves v-03 and v-04. Currently, the two models are run separately, and boundary conditions exchanged by hand until convergence (typically three iterations). The following step will be the development of a coupling platform between the two models.

The ZMS bed dynamic model is based on nonequilibrium, non-isothermal, and nonadiabatic conditions, solved with Ordinary Differential Equation (ODE) solvers [19,20]. The model is based on the following assumptions [1]: fluid plug flow with axial dispersion, negligible pressure drops, constant fluid velocity, single adsorbate system, negligible radial temperature, concentration and velocity profiles, negligible axial conduction by the column wall, ideal gas law applies for vapor phase, and uniform spherical particles.

The column is divided in several elements, defined by the user, and equations are solved each time step for each element. The model solves the following five differential equations, representing the adsorbate mass balances within gas (Eq. (3)) and solid (Eq. (4)) phases and the energy balance around the gas phase (Eq. (5)), the solid phase (Eq. (6)), and the column walls (Eq. (7)).

$$\frac{\partial c}{\partial t} = D_{ax}\frac{\partial^2 c}{\partial z^2} - \frac{u_{sup}}{\varepsilon_b}\frac{\partial c}{\partial z} - \frac{\rho_b}{\varepsilon_b\ \rho_{He}}\frac{M_{He}}{1000}\frac{\partial q}{\partial t} \tag{3}$$

$$\frac{\partial q}{\partial t} = k_{LDF}(q^* - q) \tag{4}$$

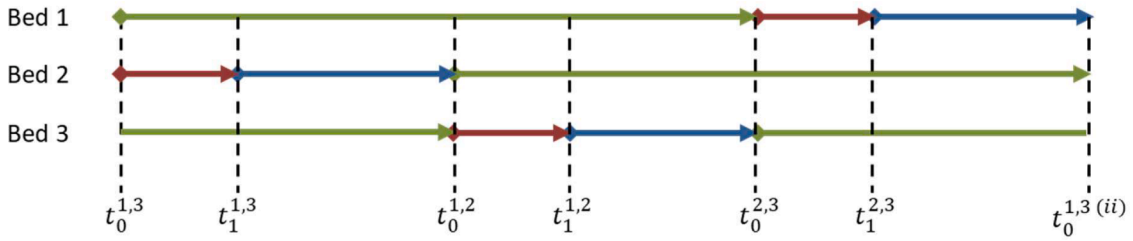


**Fig. 2.** Schematic operational mode of a system composed of three ZMS beds: adsorption (green), regeneration (red), and standby (blue).

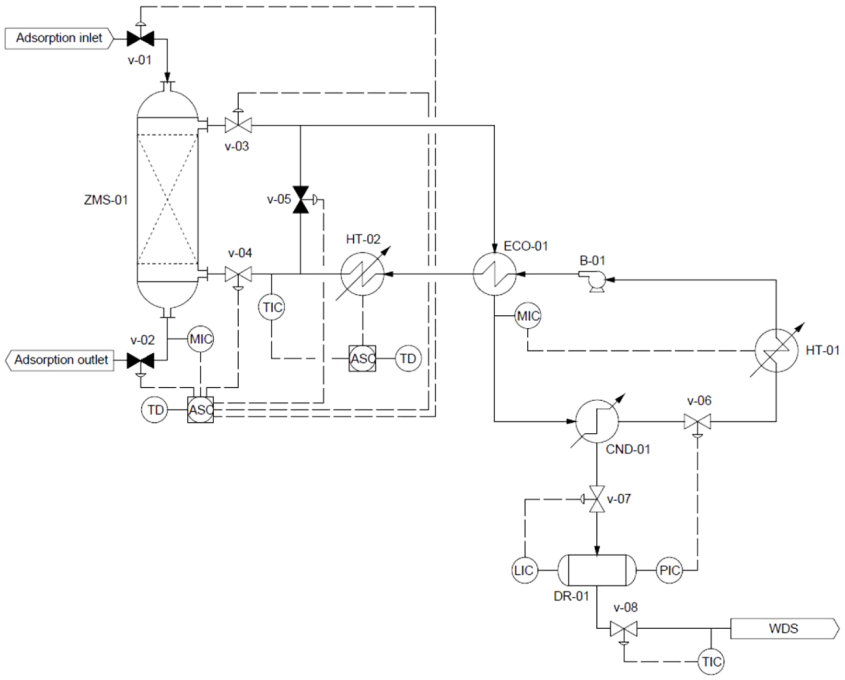


**Fig. 3.** Process Flow Diagram of the ZMS regeneration loop.

**Table 3**
Main features of heat exchangers.

| Parameter | Unit | ECO-01 | CND-01 | HT-01 | HT-02 |
|---|---|---|---|---|---|
| # tubes/pins | – | 70 | 2446 | 7 | 7 |
| # passes | – | 5 | 4 | 1 | 1 |
| Tube/pin OD | m | 0.0103 | 0.0171 | 0.0318 | 0.0318 |
| Tube/pin length | m | 1.5 | 4.6 | 0.5 | 1.0 |

$$\frac{\partial T_g}{\partial t} = \frac{k_{He}}{\rho_{He}\ c_{p,He}}\frac{\partial^2 T_g}{\partial z^2} - \frac{u_{sup}}{\varepsilon_b}\frac{\partial T_g}{\partial z} - h_{gs}\frac{\alpha_p(1-\varepsilon_b)}{\varepsilon_b\ \rho_{He}\ c_{p,He}}\left(T_g - T_s\right) - h_{gw}\frac{4}{D_c\ \varepsilon_b\ \rho_{He}\ c_{p,He}}\left(T_g - T_w\right) \quad (5)$$

$$\frac{\partial T_s}{\partial t} = h_{gs}\frac{\alpha_p}{\rho_s\ c_{p,s}}\left(T_g - T_s\right) + \frac{\Delta H_{ads}}{c_{p,s}}\frac{\partial q}{\partial t} \quad (6)$$

$$\frac{\partial T_w}{\partial t} = h_{gw}\frac{\alpha_w}{\rho_w\ c_{p,w}}\left(T_g - T_w\right) - U_{en}\frac{\alpha_{in}}{\rho_w\ c_{p,w}}\left(T_g - T_{en}\right) \quad (7)$$

The mole fraction of adsorbate in gas is indicated with $c$, $q$ is the adsorbate concentration in solid phase (mol kg$^{-1}$), $q^*$ is the equilibrium loading of the adsorber (mol kg$^{-1}$), and $T$ is the temperature in Kelvin (subscripts *g, s, w*, and *en* stand for gas, particle, column wall, and environment, respectively). A complete list of the symbols, along with a detailed description of the model and its preliminary validation, are presented in annex.

In Eq. (3), the third term on the right side is the source term that accounts for the moles of adsorbate that passes from the gas phase to the solid phase. The variation of $q$ over time is calculated with Eq. (4). When positive (i.e., the concentration of adsorbate in the solid phase increases), the third term in Eq. (3) is negative, indicating that adsorbate moles pass from gas to solid phase.

Depending on the initial and boundary conditions adopted for the calculation, the ZMS dynamic model can simulate both the adsorption and regeneration modes. The set of initial conditions to be input are the initial adsorbate molar fraction in gas phase $c_0$, the initial loading of the adsorbate in the solid phase $q_0$, and the initial temperature of the gas phase $T_{g0}$, the solid phase $T_{s0}$, and the column walls $T_{c0}$. Each of these must be input for each element composing the computational domain. The boundary conditions used for the simulations are the adsorbate concentration at the column inlet, the feed mass flow rate, the gas pressure, the environmental temperature, and the heat transfer coefficient between the outside wall of the column and the environment. In addition, the geometrical features of the column in terms of dimensions and bed loading (i.e., characteristics of the zeolite pellets and the hydraulic features of the bed) must be input. The outcomes of the simulations are the profiles of the molar fraction, the temperature, and the adsorbate concentration along the column over the whole problem time assumed for the calculation. All the simulations presented in the present paper have been carried out using the ode15s MATLAB solver with a scalar relative error tolerance of $10^{-3}$, a vector of absolute error

tolerance of $10^{-6}$, and a time step of 1 s.

The thermal-hydraulic model of the regeneration loop has been developed with RELAP5/MOD3.3 (RELAP5 in the following). It is a system thermal-hydraulic code, originally developed by the U.S. Nuclear Regulatory Commission (NRC) for the transient analysis of Light Water Reactors (LWR) [21]. The code can be used to study a wide range of systems, involving different fluids. In fusion, among others, RELAP5 was used in the frame of the ITER TBM programme [22,23], for transient analysis of the EU-DEMO WCLL BB PHTS [24], and for the preliminary thermal-hydraulic analysis of the EU-DEMO HCPB BB PHTS (RELAP5–3D version for this case) [25].

The ZMS regeneration loop model consists of an overall number of 313 control volumes and 311 hydraulic junctions, simulating all the elevation changes preliminary assumed for the loop. Furthermore, an overall number of 132 heat structures is used to reproduce the heat transfer occurring in the ECO-01, the CND-01, the HT-01 and HT-02. The heat losses towards environment are neglected in this preliminary phase. The ECO-01 and CND-01 are passive components in which heat transfer is computed between the fluids flowing in the hot and cold side of each heat exchanger. On the other hand, the power provided by the two heaters is calculated at each time step by the control system, implemented in the model through Proportional-Integral-Derivative controllers.

## 4. Results

The results presented in this section have been obtained after three iterations between the two computational domains. The RELAP5 results are presented from Figs. 4 to 7 where white background represents the regeneration phase and the light blue is the standby condition (please, refer to the online version of the paper for coloured figures). The initial conditions of the regeneration loop are derived from a preliminary steady state simulation. Boundary conditions are the inlet conditions of the stream coming from v-03 (i.e., pressure, temperature, and composition) and the cold side conditions at the condenser, that are a water flow rate of 164 kg $s^{-1}$ at 15 °C and 1.5 bar. The time step adopted for the simulation is $10^{-2}$ s, derived from a time step sensitivity analysis in the range of $10^{-2}$ – $10^{-3}$ s.

Fig. 4 presents the $Q_2O$ molar fraction in the mixture stream calculated in six relevant positions in the regeneration loop. Simulation starts with an initial baseline $Q_2O$ concentration of 5.8 $10^{-3}$, representing the residual content of the previous phase. When v-03 and v-04 open and simultaneously, v-05 closes, a mixture flow rate of 0.0973 kg $s^{-1}$ feeds the ZMS bed. The mixture, kept at 85 °C during the standby, is heated up to 300 °C by the HT-02, as shown by the yellow line in Fig. 5. The bed is gradually heated and regenerated (see results of the ZMS dynamic model in the following). Therefore, the $Q_2O$ content in the throughput coming from the ZMS-01 increases, as shown in Fig. 4 where the black and green lines overlapping, proving that no condensation occurs inside the ECO-01. The $Q_2O$ content drops at the CND-01 outlet and is collected in the DR-01 (see Fig. 7), whereas the residual humidity moves through the loop remaining quite uniform until the ZMS-01. The residual $Q_2O$ molar fraction reaches a first plateaux to 0.015 during the first two hours due to the large release from the ZMS-01 and then, when the adsorber bed is almost regenerated, decreases again to the baseline value. At the same time, the temperatures stabilize to a quasi-steady state condition. The yellow lines (ZMS-01 inlet) represent the output of the RELAP5 simulation, assumed as boundary condition for the MATLAB calculation. Fig. 6 presents the CND-01 power removal and the HT-01 and HT-02 power supply. In the first two hours, due to the high $Q_2O$ content, the CND-01 power removal increases up to a peak of around 170 kW. Most of the humidity is condensed and collected into DR-01 and the CND-01 outlet temperature (i.e., HT-01 inlet temperature in Fig. 5) reaches the minimum value of 100 °C. At the same time, HT-01 prevent condensation into the ECO-01, turning off at 2 h, and HT-02 guarantees an inlet temperature of the ZMS-01 of 300 °C, reaching a peak power of around 90 kW in the first minutes of the regeneration. When the quasi-steady state conditions are reached (5 h), the HT-02 balances the CND-01 heat removal. It is worth mentioning that heat losses through the walls of pipes and components are currently not considered in the model. The ZMS-01 can be considered regenerated after 8 h from the beginning of the transient and the standby phase starts with the closure of v-03 and v-04 close and the opening of v-05. HT-02 turns off and the loop is brought to the standby temperature of 85 °C. The baseline $Q_2O$ molar fraction is 5.8 $10^{-3}$ (see Fig. 4), corresponding to a partial pressure of 46.4 kPa. The amount of $Q_2O$ collected inside the DR-01 is presented in Fig. 7, preliminary assuming that it is not delivered to the WDS. At the end of the regeneration phase, 1.78 kg of tritiated water (100 Ci $kg^{-1}$) is recovered, increasing to 1.8 kg during the standby, which corresponds to 0.0185 and 0.0187 g of tritium (around 178 Ci). The baseline tritium inventory in the loop during the standby is 73 Ci,

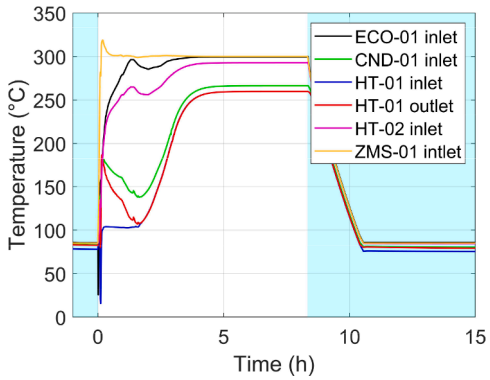


**Fig. 5.** RELAP5 simulation: Temperature in relevant monitored points.

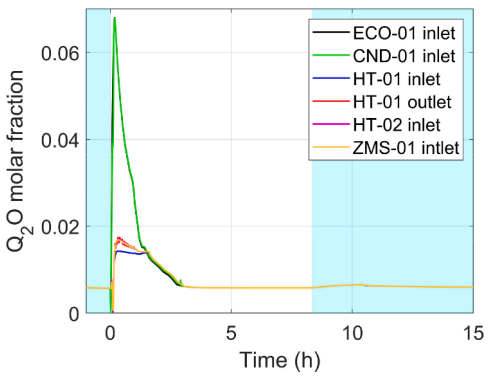


**Fig. 4.** RELAP5 simulation: $Q_2O$ content in relevant monitored points.

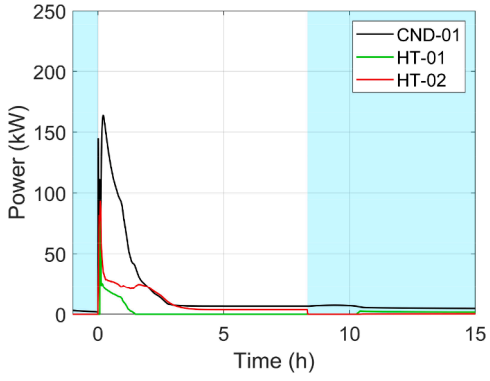


**Fig. 6.** RELAP5 simulation: CND-01 power removal and HT-01 and HT-02 power supply.

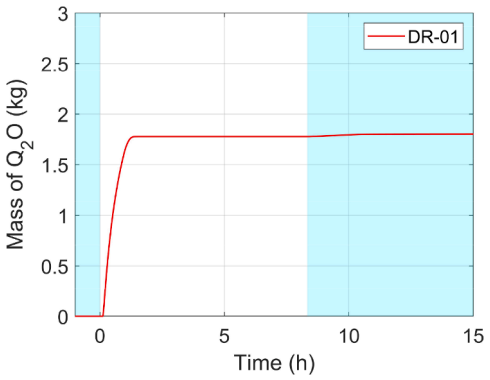


**Fig. 7.** RELAP5 simulation: mass of $Q_20$ collected inside the drum.

considering volumes of pipeline and components.

The water molar fraction and the temperature of the mixture, calculated by RELAP5 at the ZMS-01 inlet (yellow lines in Figs. 4 and 5) are used as boundary conditions for the MATLAB simulation of the ZMS regeneration. The main results of this analysis are reported in Figs. 8, 9, and 10 for three relevant position inside the bed i.e., inlet (yellow line), middle (red) and outlet (black), being this latter the boundary condition for the RELAP5 calculation. Initial conditions of the bed have been evaluated with a preliminary simulation of the adsorption phase, obtaining an equilibrium loading of $Q_2O$ into the ZMS pellets of 11.08 mol $kg^{-1}$ and an initial temperature of the zeolite material of 25 °C.

Fig. 8 shows the $Q_2O$ molar fraction in the gas phase along the adsorber bed, supposing the beginning of the regeneration transient at 0 h. Yellow line is the boundary condition provided by RELAP5, with an initial increase up to 0.02 and the following decrease to the baseline value. While the purge mixture moves along the ZMS-01, water is released from the zeolite material with a rate depending on operative conditions. The $Q_2O$ molar fraction in the gas phase quickly increases at the beginning of the regeneration process, reaching the maximum of 0.0679 at 0.07 h (see Fig. 8). At this time, the regeneration involves the whole bed and the $Q_2O$ sorbens loading starts to decrease faster (Fig. 9), leading to a lower release rate and the consequent reduction of the $Q_2O$ molar fraction in the gas phase (Fig. 8). At around 0.5 h, the $Q_2O$ release stops in the middle of the bed, affected by the increase of the $Q_2O$ molar fraction in the inlet purge mixture. The same occurs at the outlet of the bed with a delay of around half an hour. After that, the $Q_2O$ content in the inlet stream decreases to the baseline value and the $Q_2O$ sorbens loading reduces again to the final value. A quasi-steady state condition is reached after 4 h from the beginning of the regeneration and the process can be considered concluded at 8 h. The temperature trend is presented in Fig. 10. The bed, initialized at 25 °C, is heated by the purge mixture entering at 300 °C. The desorption reaction is an endothermic process

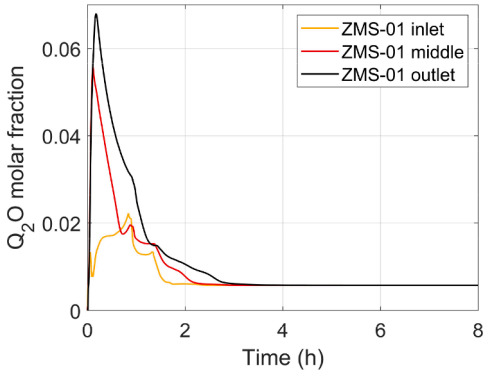


**Fig. 8.** MATLAB simulation of the regeneration transient: $Q_2O$ molar fraction in the gas phase at the ZMS-01 outlet.

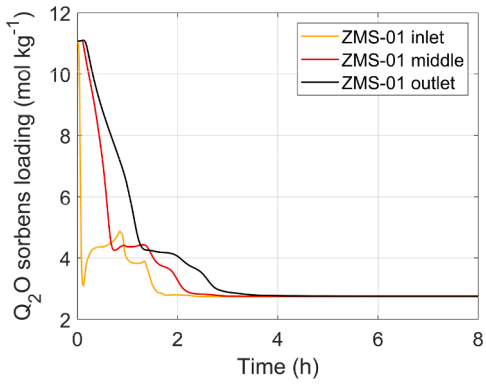


**Fig. 9.** MATLAB simulation of the regeneration transient: $Q_2O$ sorbens loading in three relevant positions of ZMS-01.

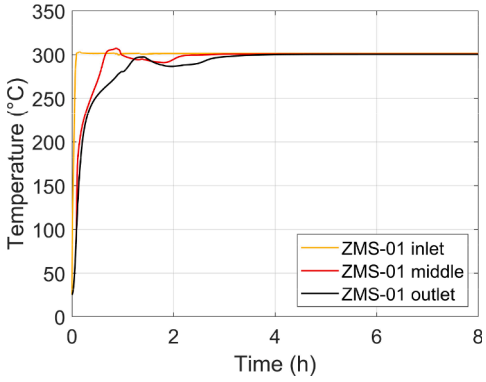


**Fig. 10.** MATLAB simulation of the regeneration transient: gas temperature in three relevant positions of ZMS-01.

and thus, the bed heating proceeds slower. The ZMS-01 can be considered regenerated when all the zeolite material reaches the temperature of 300 °C i.e., the desorption of water stops. Due to the baseline $Q_2O$ molar fraction in the inlet purge mixture, and the consequent residual loading of 2.76 mol $kg^{-1}$, the regeneration efficiency ensured by the described procedure is 74.4 %, leading to a tritium immobilization inside each bed of 0.153 g.

Referring to Fig. 2, the characteristic times obtained by the computational activity are summarized in Table 4. The duration of the adsorption phase (60 h) has been evaluated with a proper simulation with MATLAB model.

## 5. Conclusions

The Coolant Purification System represents one of the mitigation strategies to prevent the rise of the tritium concentration in the EU-DEMO primary coolant loop above a fixed target. Copper Oxide and Zeolite Molecular Sieve beds are the main technologies adopted in helium CPS however, to operate the CPS loop, auxiliary components (e.g., heat exchangers) are essential. Firstly, the paper has presented the advanced design of helium CPS, and then has described the model developed to study the regeneration process of the ZMS bed. Indeed, the model is composed of two different and separated tools, one in MATLAB to assess the main features inside the ZMS column and one in RELAP5 to

**Table 4**
Characteristic times (h) of the proposed ZMS regeneration procedure.

| $t_0^{1,3}$ | $t_1^{1,3}$ | $t_0^{1,2}$ | $t_1^{1,2}$ | $t_0^{2,3}$ | $t_1^{2,3}$ | $t_0^{1,3\ (ii)}$ |
|---|---|---|---|---|---|---|
| 0 | 8 | 30 | 38 | 60 | 68 | 90 |

describe the regeneration loop.

Outcomes of the RELAP5 simulations provide the $Q_2O$ content and the temperature in relevant monitored points of the loop, the power required from several components and the $Q_2O$ amount collected in the drum to be sent to the Water Detritiation System. Another important information is given from the residual $Q_2O$ molar fraction at the end of the regeneration loop, from which is possible to assess the tritium inventory in the loop and to define the actual initial $Q_2O$ concentration in the purge gas entering the ZMS during the regeneration. Given the helium CPS regeneration loop features described in the paper, the residual $Q_2O$ molar fraction is 5.8 $10^{-3}$, corresponding to a partial pressure of 46.4 kPa, the amount of $Q_2O$ collected inside the drum at the end of the regeneration phase is 1.78 kg (100 Ci $kg^{-1}$), increasing to 1.8 kg during the standby, while the baseline tritium inventory in the loop during the standby is 73 Ci. Considering the residual $Q_2O$ molar fraction in the regeneration loop as inlet condition in the helium purge gas and using the MATLAB tool, main features of the ZMS column during the regeneration have ben assessed. It has been possible to establish that a quasi-steady state condition is reached after 4 h from the beginning of the regeneration and the process can be considered concluded at 8 h, the ZMS residual loading is 2.76 mol $kg^{-1}$, the regeneration efficiency is 74.4 %, leading to a tritium immobilization inside each bed of 0.153 g.

Literature provides many activities, analytical and experimental, describing the adsorption/desorption behaviour of ZMS beds. However, this work differs from the others because it integrates also the features of the regeneration loop giving a more realistic estimation of the entire process performances. Currently the results of one simulation tool are used as input for the other, a better interface integration will be a topic of future activities.

## CRediT authorship contribution statement

**Vincenzo Narcisi:** Conceptualization, Methodology, Software, Validation, Formal analysis, Investigation, Data curation, Writing – original draft, Writing – review & editing, Visualization. **Alessia Santucci:** Conceptualization, Resources, Data curation, Writing – original draft, Writing – review & editing, Visualization, Supervision, Project administration, Funding acquisition.

## Declaration of competing interest

The authors declare that they have no known competing financial interests or personal relationships that could have appeared to influence the work reported in this paper.

## Data Availability

No data was used for the research described in the article.

## Acknowledgements

This work has been carried out within the framework of the EUROfusion Consortium, funded by the European Union via the Euratom Research and Training Programme (Grant Agreement No 101052200 — EUROfusion). Views and opinions expressed are however those of the author(s) only and do not necessarily reflect those of the European Union or the European Commission. Neither the European Union nor the European Commission can be held responsible for them.

## Appendix

This appendix reports a detailed description of coefficients and parameters adopted in the ZMS dynamic model. The list of symbols involved in the differential equations presented in Section 3.1, along with the unit and their descriptions, are reported in Table A1.

The axial diffusion coefficient is calculated with Eq. (A1) [26]:

$$\frac{\varepsilon_b D_{ax}}{D_M} = 20 + 0.5\ Sc\ Re \tag{A1}$$

Where $D_M$ is the molecular diffusion coefficient ($m^2\ s^{-1}$), $Sc$ is the Schmidt number, and $Re$ the Reynolds number. The molecular diffusion coefficient is calculated by the Fuller equation [27]:

$$D_M = 1.013\ 10^{-7}\ T_g^{1.75} \frac{\left(\frac{1}{M_{H_2O}} + \frac{1}{M_{He}}\right)^{0.5}}{p\left(Dv_{H_2O}^{1/3} + Dv_{He}^{1/3}\right)^2} \tag{A2}$$

here $Dv_{H2O}$ and $Dv_{He}$ are the water and helium diffusion volumes equal 12.7 and 2.88, respectively.

The variation of $q$ over time depends on the difference between the equilibrium loading $q^*$ and the adsorbate concentration in the solid phase, representing the driving force for the adsorption (in case of positive difference) and for the regeneration (in case of negative difference). The variation of adsorbate concentration in solid phase is modelled by the Linear Driving Force (LDF) approach through $k_{LDF}$, calculated as [19,20]:

$$k_{LDF} = \left(\frac{\rho_s}{k_f\ \rho_{He}\ \alpha_p}\ \frac{q^*}{c} + \frac{D_p}{10\ D_{ps}\ \alpha_p}\right)^{-1} \tag{A3}$$

Where $k_f$ is the film mass transfer coefficient ($m\ s^{-1}$), $D_p$ is the particle diameter (m), and $D_{ps}$ is the effective particle diffusion coefficient ($m^2\ s^{-1}$). $k_f$ is calculated by Eq. (A4) [26]:

$$Sh = \frac{D_p\ k_f}{D_m} = 2 + 1.1\ Re^{0.6}\ Sc^{1/3} \tag{A4}$$

Where $Sh$ is the Sherwood number. $D_{ps}$ is evaluated with Eq. (A5) [20]:

$$D_{ps} = D_s + D_K \frac{\varepsilon_p\ \rho_g}{\rho_p} \frac{\partial c^*}{\partial q} \tag{A5}$$

Where $c^*$ is the mole fraction of adsorbate in gas phase at equilibrium with $q$, $\varepsilon_p$ is the particle porosity, $D_s$ is the surface diffusion coefficient ($m^2\ s^{-1}$), and $D_K$ is the Knudsen diffusion coefficient ($m^2\ s^{-1}$). $D_s$ and $D_K$ are evaluated with Eq. (A6) and A7, respectively:

$$D_s = \frac{1.61\ 10^{-6}}{\tau_s} e^{-\frac{E}{R\ T}} \tag{A6}$$

$$D_K = 9.7\ 10^{-9} \frac{r_e}{\tau_p} \left( \frac{T_g}{M_{H_2O}} \right)^{0.5} \tag{A7}$$

Where $\tau_s$ and $\tau_p$ are the superficial and pore tortuosity factors, respectively, $E$ is the surface diffusion activation energy ($J\ mol^{-1}$), $R$ is the gas constant ($J\ mol^{-1}\ K^{-1}$), and $r_e$ is the mean porous radius (Å).

The equilibrium loading $q^*$ strictly depends on the adsorbent material. For the zeolite 4A pellets, an empirical law based on Langmuir model is derived by Wang [2]:

$$q^*_{Q2O} = \frac{q_a b_a p_{Q_2O}}{1 + b_a p_{Q_2O}} + \frac{q_\beta b_\beta p_{Q_2O}}{1 + b_\beta p_{Q_2O}} \tag{A8}$$

Where coefficients $b_{\alpha,\beta,}$ are calculated as function of material temperature, following an Arrhenius type dependency:

$$b_{\alpha,\beta} = b_{\alpha,\beta,0} e^{\frac{E_{\alpha,\beta}}{RT}} \tag{A9}$$

Table A2 collects the parameter for the dual site Langmuir model for the zeolite 4A pellets.

Focusing on energy balance equations, $h_{gs}$ [26] and $h_{gw}$ [28] are calculated through the following expressions of the Nusselt number ($Nu$):

$$Nu = \frac{h_{gs}\ D_p}{k_{He}} = 2 + 1.1\ Re^{0.6}\ Pr^{1/3} \tag{A10}$$

$$Nu = \frac{h_{gw}\ D_p}{k_{He}} = 0.6\ Re^{0.5}\ Pr^{1/3} \tag{A11}$$

Where $Pr$ is the Prandtl number. $U_{en}$, representing the overall heat transfer coefficient from the gas phase to the environment, is calculated assuming an insulation of the column.

The main assumptions adopted in the model, along with the main references, are summarized in Table A3.

**Table A1**
List of symbols.

| Symbol | Unit | Description |
|---|---|---|
| $c$ | – | Mole fraction of adsorbate in gas phase |
| $D_{ax}$ | $m^2\ s^{-1}$ | Axial diffusion coefficient |
| $u_{sup}$ | $m\ s^{-1}$ | Superficial gas velocity |
| $\varepsilon_b$ | – | Bed void fraction |
| $\rho_b$ | $kg\ m^{-3}$ | Bed density |
| $\rho_{He}$ | $kg\ m^{-3}$ | Helium density |
| $c_{p,He}$ | $J\ kg^{-1}\ K^{-1}$ | Helium specific heat |
| $k_{He}$ | $W\ m^{-1}\ K^{-1}$ | Helium thermal conductivity |
| $M_{He}$ | $g\ mol^{-1}$ | Helium molecular weight |
| $q$ | $mol\ kg^{-1}$ | Adsorbate concentration in solid phase |
| $q^*$ | $mol\ kg^{-1}$ | Equilibrium loading |
| $k_{LDF}$ | $s^{-1}$ | Overall mass transfer coefficient |
| $T_g$ | K | Gas temperature |
| $T_s$ | K | Particle temperature |
| $T_w$ | K | Column wall temperature |
| $T_{en}$ | K | Environment temperature |
| $z$ | m | Axial position in the bed |
| $D_c$ | m | Column diameter |
| $h_{gs}$ | $W\ m^{-2}\ K^{-1}$ | Gas-particle heat transfer coefficient |
| $h_{gw}$ | $W\ m^{-2}\ K^{-1}$ | Gas-column wall heat transfer coefficient |
| $\alpha_p$ | $m^{-1}$ | Particle external surface to volume ratio |
| $\alpha_w$ | $m^{-1}$ | Column external surface to volume ratio |
| $\alpha_{in}$ | $m^{-1}$ | Insulation external surface to volume ratio |
| $\rho_s$ | $kg\ m^{-3}$ | Particle density |
| $c_{p,s}$ | $J\ kg^{-1}\ K^{-1}$ | Particle specific heat |
| $\rho_w$ | $kg\ m^{-3}$ | Column wall density |
| $c_{p,w}$ | $J\ kg^{-1}\ K^{-1}$ | Column wall specific heat |
| $\Delta H_{ads}$ | $J\ mol^{-1}$ | Heat of adsorption of adsorbate |
| $U_{en}$ | $W\ m^{-2}\ K^{-1}$ | Overall heat transfer coefficient for column |

**Table A2**
Fitted Langmuir parameters for water on SYLOBEAD 4A.

| Parameter | Unit | Value |
|---|---|---|
| $q_\alpha$ | mol $kg^{-1}$ | 9.57 |
| $q_\beta$ | mol $kg^{-1}$ | 1.59 |
| $b_\alpha$ | $bar^{-1}$ | 2.02 $10^{-6}$ |
| $b_\beta$ | $bar^{-1}$ | 3.24 $10^{-3}$ |
| $E_\alpha$ | kJ $mol^{-1}$ | 56.86 |
| $E_\beta$ | kJ $mol^{-1}$ | 53.50 |

**Table A3**
Main parameters assumed for the dynamic simulation of ZMS beds.

| Parameter | Unit | Value | Reference |
|---|---|---|---|
| Pore tortuosity factor, $\tau_p$ | – | 4 | [29] |
| Superficial tortuosity factor, $\tau_s$ | – | 4 | [29] |
| Particle porosity, $\epsilon_p$ | – | 0.53 | [14] |
| Heat of adsorption of water, $\Delta H_{ad}$ | J $mol^{-1}$ | 54 961 | [30] |
| Surface diffusion activation energy, $E$ | J $mol^{-1}$ | 0.45 $\Delta H_{ads}$ | [31] |
| Insulator thermal conductivity | W $m^{-1} K^{-1}$ | 0.023 | – |

A preliminary validation procedure has been carried out with experimental data available in literature. Among these, only the work presented by Gorbach et al. [30] provides experimental data on the breakthrough curves of molar fraction of water (even if only for the adsorption phase) with enough information regarding operative conditions. The description of the experimental apparatus, along with geometrical features of the packed bed, are collected in [30]. The experiments adopt synthetic air as carrier gas and the water content is obtained mixing a proper throughput of hydrogen with the carrier gas flow rate and then, oxidizing all the $H_2$ content. The error of the moisture content is declared to be less than 1 %. The column is filled with zeolite 4A pellets [30].

Four tests are considered for the validation procedure. A breakthrough curve of molar fraction of water at the bed outlet are available for each test whereas breakthrough curve of gas temperature is available only for case A. Boundary conditions of each test are summarized in Table A4 [30].

**Table A4**
Experimental parameters adopted as boundary conditions for simulations.

| Parameter | Unit | Test A | Test B | Test C | Test D |
|---|---|---|---|---|---|
| Water molar fraction | ppm | 4594 | 4410 | 4603 | 4531 |
| Flow rate | Nl $min^{-1}$ | 1.84 | 1.998 | 2.00 | 1.98 |
| Pressure | bar | 5.0 | 2.0 | 2.0 | 2.0 |
| W all temperature | °C | 30 | 30 | 50 | 80 |

The simulation results are compared with experimental data in Fig. A1 and Fig. A2 for the breakthrough curves of water molar fraction and gas temperature, respectively. Although some discrepancies between the experiment and the simulations, the dynamic model has provided satisfactory results in the prediction of the time required for saturation and of the final conditions after the breakthrough occurring for different operative conditions. Indeed, the delay of the breakthrough going from test D to A is well assessed by the code. Nevertheless, the kinetic of the adsorption reaction seems to be overestimated by the model, obtaining curves steeper than the experiments. On the other hand, referring to test A, the breakthrough curve of the gas temperature suggests an opposite conclusion. As a matter of fact, the contribution of the heat of adsorption is proportional to the adsorption rate (i.e., the variation of $q$ over time). Thus, an overestimation of the adsorption rate should lead to an over prediction of the gas temperature. In Figure A. 2 the temperature increase is well reproduced by the model until 24 h from the beginning of the test. It could lead to the conclusion that the first phase of the adsorption rate is well simulated. However, the major discrepancies in the breakthrough curves of water molar fraction are observed in the first minutes of the breakthrough occurrence for the test A. On the other hand, when discrepancies occur in the gas temperature breakthrough, they are less visible in the water molar fraction breakthrough.

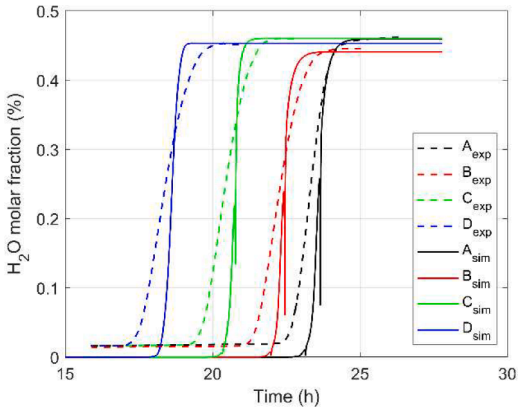


**Fig. A1.** Breakthrough curves of molar fraction of water for case A, B, C, and D: experimental results (dashed lines) and simulation results (solid lines).

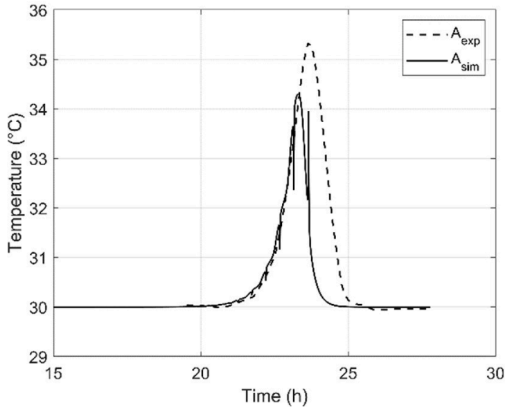


**Fig. A2.** Breakthrough curve of gas temperature for case A: experimental results (dashed lines) and simulation results (solid lines).

It is worth emphasizing that the model is based on some assumed parameters (e.g., superficial and pore tortuosity factors) and that experimental data, although well reported in [30], miss relevant information regarding experimental uncertainties and have limited number of significant digits in the boundary conditions, especially regarding water molar fraction and volumetric flow rate. As shown in Figure A. 1, the experimental apparatus seems not able to acquire data for low water molar fraction, reporting a lower value of around 0.02 %, when 0 % is expected. Furthermore, the distance between the column outlet and the acquisition points, for both the water molar fraction and the gas temperature, could plays a relevant role in the discrepancy between simulations (the parameters are evaluated within the last element of the column) and the experiments. Thus, this comparison represents the first step of a validation procedure that must pass through an optimization of the model and a comparison with other experimental data (e.g., future HYDREX experiments at ENEA laboratories).

## References

[1] S. Jovic, Y. Laxminarayan, J. Keurentjes, J. Schouten, J. van der Schaaf, Adsorptive Water Removal from Dichloromethane and Vapor-Phase Regeneration of a Molecular Sieve 3A Packed Bed, Ind. Eng. Chem. Res. 56 (2017) 5042–5054, https://doi.org/10.1021/acs.iecr.7b00433.

[2] Y. Wang, Measurements and Modeling of Water Adsorption Isotherms of Zeolite Linde-Type A Crystals, Ind. Eng. Chem. Res. 59 (2020) 8304–8314, https://doi.org/10.1021/acs.iecr.9b06891.

[3] S. Mokhatab, W.A. Poe, J.Y. Mak, Natural Gas Dehydration and Mercaptans Removal, in: S. Mokhatab, W.A. Poe, J.Y. Mak (Eds.), Handbook of Natural Gas Transmission and Processing, 4th ed., Gulf Professional Publishing, Elsevier, Waltham, MA, 2019, p. 307. Chapter 9.

[4] H.L. Bart, U. von Gemmingen, Ullmann's Encyclopedia of Industrial Chemistry, Wiley–VCH, Weinheim, Germany, 2005, https://doi.org/10.1002/14356007.b03_09.pub2.

[5] A.I. Parracho, D. Demange, S. Knipe, L.T. Le, K.H. Simon, S. Welte, Processing highly tritiated water desorbed from molecular sieve bed using PERMCAT, Fusion Eng. Des. 7-8 (2012) 1277–1281, https://doi.org/10.1016/j.fusengdes.2012.02.118.

[6] G. Federici, Testing needs for the development and qualification of a breeding blanket for DEMO, Nucl. Fusion 63 (2023) 125002, https://doi.org/10.1088/1741-4326/ad00cb.

[7] V. Narcisi, A. Quartararo, I. Moscato, A. Santucci, Analysis of Coolant Purification Strategies for Tritium Control in DEMO Water Primary Coolant, Energies 16 (2023) 617, https://doi.org/10.3390/en16020617.

[8] A. Santucci, M. Incelli, L. Noschese, C. Moreno, F. Di Fonzo, M. Utili, S. Tosti, C. Day, The issue of Tritium in DEMO coolant and mitigation strategies, Fusion Eng. Des. 158 (2020) 111759, https://doi.org/10.1016/j.fusengdes.2020.111759.

[9] C. Day, K. Battes, B. Butler, S. Davies, L. Farina, A. Frattolillo, R. George, T. Giegerich, S. Hanke, T. Hartl, Y. Igitkhanov, T. Jackson, N. Jayasekera, Y. Kathage, P.T. Lang, R. Lawless, X. Luo, C. Neugebauer, B. Ploeckl, A. Santucci, J. Schwenzer, T. Teichmann, T. Tijssen, S. Tosti, S. Varaoutis, A. Vazquez Cortes, The pre-concept design of the DEMO tritium, matter injection and vacuum systems, Fusion Eng. Des. 179 (2022) 113139, https://doi.org/10.1016/j.fusengdes.2022.113139.

[10] F.A. Hernandez, P. Arena, L.V. Boccaccini, I. Cristescu, A. Del Nevo, P. Sardain, G. A. Spagnuolo, M. Utili, A. Venturini, G. Zhou, Advancements in Designing the DEMO Driver Blanket System at the EU DEMO Pre-Conceptual Design Phase: overview, Challenges and Opportunities, J. Nucl. Eng. 4 (2023) 565–601, https://doi.org/10.3390/jne4030037.

[11] J.C. Schwenzer, A. Santucci, C. Day, Modeling of the HCPB Helium Coolant Purification System for EU-DEMO: process Simulations of Molecular Sieves and NEG Sorbents, Fusion Sci. Tech. 79 (2023) 1208–1218, https://doi.org/10.1080/15361055.2023.2189550.

[12] I. Moscato, L. Barucca, E. Bubelis, G. Caruso, S. Ciattaglia, C. Ciurluini, A. Del Nevo, P.A. Di Maio, F. Giannetti, W. Hering, P. Lorusso, E. Martelli, V. Narcisi, S. Norrman, T. Pinna, S. Perez-Martin, A. Quartararo, M. Szogradi, A. Tarallo, E. Vallone, Tokamak cooling systems and power conversion system options, Fusion Eng. Des. 178 (2022) 113093, https://doi.org/10.1016/j.fusengdes.2022.113093.

[13] J.A. Rodriguez, J.Y. Kim, J.C. Hanson, M. Perez, A.I. Frenkel, Reduction of CuO in $H_2$: in Situ Time-Resolved XRD Studies, Catal. Lett. 85 (2003) 247–254, https://doi.org/10.1023/A:1022110200942.

[14] S. Tosti, A. Santucci, I. Cristescu, S. Bassini, D. Diamanti, M. Utili. Report review of gas treatment technologies. Tech. Rep. TRANSAT D1.3, 2019.
[15] C. Moreno, F.R. Urgorri, Analyses of HCPB and WCLL for the review meeting, EUROfusion Tech. Rep. (2021). BB-6.2.1-T005-D001 EFDA_D_2PLELC.
[16] V. Narcisi, A. Santucci, Water distillation for coolant purification system of DEMO water-cooled lithium lead breeding blanket, Fusion Eng. Des. 190 (2023) 113547, https://doi.org/10.1016/j.fusengdes.2023.113547.
[17] S. Ergun, Fluid flow through packed columns, J. Chem. Eng. 48 (1952) 89–94.
[18] The American Society of Mechanical Engineers (ASME), Boiler and Pressure Vessel Code, Section III, Division 1, Subsection NC, 3324.3, New York, 2015.
[19] J.M. Schork, J.R. Fair, Parametric Analysis of Thermal Regeneration of Adsorption Beds, Ind. Eng. Chem. Res. 27 (1988) 457–469, https://doi.org/10.1021/ie00075a016.
[20] B. Ambrozek, The Simulation of Cyclic Thermal Swing Adsorption (TSA) Process, in: W. Mitkowski, J. Kacprzyk (Eds.), Modelling Dynamics in Processes and Systems, Scientific Publishing Servies Pvt. Ltd., Chennai, 2009, pp. 165–178.
[21] USNRC, RELAP5/MOD3 Code Manual Volume I: code Structure, System Models, and Solution Methods, NUREG/CR-5535, Washington DC, 1998.
[22] C. Ciurluini, V. Narcisi, A. Tincani, C. Ortiz Ferrer, F. Giannetti, Conceptual design overview of the ITER WCLL Water Cooling System and supporting thermal-hydraulic analysis, Fusion Eng. Des. 171 (2021) 112598, https://doi.org/10.1016/j.fusengdes.2021.112598.
[23] L. Melchiorri, V. Narcisi, C. Ciurluini, F. Giannetti, G. Caruso, A. Tassone, Preliminary MHD pressure drop analysis for the prototypical WCLL TBM with RELAP5/MOD3.3, Fusion Eng. Des 176 (2022) 113048, https://doi.org/10.1016/j.fusengdes.2022.113048.
[24] C. Ciurluini, M. D'Onorio, F. Giannetti, G. Caruso, A. Del Nevo, Transient analysis of a locked rotor/shaft seizure accident involving the EU-DEMO WCLL Breeding Blanket primary cooling circuits, Fusion Eng. Des. 187 (2023) 113396, https://doi.org/10.1016/j.fusengdes.2022.113396.
[25] S. D'Amico, P.A. Di Maio, X.Z. Jin, F.A. Hernandez Gonzalez, I. Moscato, G. Zhou, Preliminary thermal-hydraulic analysis of the EU-DEMO Helium-Cooled Pebble Bed fusion reactor by using the RELAP5-3D system code, Fusion Eng. Des. 162 (2021) 112111, https://doi.org/10.1016/j.fusengdes.2020.112111.
[26] N. Wakao, T. Funazkri, Effect of fluid dispersion coefficients on particle-to-fluid mass transfer coefficients in packed beds, Chem. Eng. Sci. 33 (1978) 1375–1384, https://doi.org/10.1016/0009-2509(78)85120-3.
[27] E. Fuller, Diffusion of halogenated hydrocarbons in helium. The effect of structure on collision cross sections, J. Phys. Chem. 73 (1987) 3679–3685, https://doi.org/10.1021/j100845a020.
[28] A.G. Dixon, D.L. Cresswell, Theoretical Prediction of Effective Heat Transfer Parameters in Packed Beds, AlChe Journal 25 (4) (1979) 663–676, https://doi.org/10.1002/aic.690250413.
[29] C.N. Satterfield, Mass Transfer in Heterogeneous Catalysis, in E. Robert, Krieger: huntington, NY, 1981.
[30] A. Gorbach, M. Stegmaier, G. Eigenberger, Measurement and Modeling of Water Vapor Adsorption on Zeolite 4A – Equilibria and Kinetics, Adsorption 33 (2004) 1375–1384, https://doi.org/10.1023/B:ADSO.0000024033.60103.ff.
[31] K.J. Sladek, E.R. Gilliland, R.F. Baddour, Diffusion on Surfaces. II. Correlation of Diffusivities of Physically and Chemically Adsorbed Species, Ind. Rng. Chem. Fundamen 13 (2) (1974) 100–105, https://doi.org/10.1021/i160050a002.